# Diffusion imaging of the vertebral bone marrow

Olaf Dietrich[1], Tobias Geith[2], Maximilian F. Reiser[1,2], Andrea Baur-Melnyk[2]

[1] Josef Lissner Laboratory for Biomedical Imaging, Institute for Clinical Radiology, Ludwig-Maximilians-University Hospital Munich, Germany

[2] Institute for Clinical Radiology, Ludwig-Maximilians-University Hospital Munich, Germany

Review article for special issue "Diffusion magnetic resonance imaging outside the brain"



Final version: NMR Biomed (2015, epub ahead of print). <URL:http://dx.doi.org/10.1002/nbm.3333>

## Abstract

Diffusion-weighted magnetic resonance imaging (DWI) of the vertebral bone marrow is a clinically important tool for the characterization of bone-marrow pathologies and, in particular, for the differentiation of benign (osteoporotic) and malignant vertebral compression fractures.

DWI of the vertebral bone marrow is, however, complicated by some unique magnetic resonance and tissue properties of vertebral bone marrow. Due to both the spongy microstructure of the trabecular bone and the neighborhood of the lungs, soft tissue, or large vessels, substantial magnetic susceptibility variations occur which severely reduce the magnetic field homogeneity as well as the transverse relaxation time $T_2^*$, and, thus, complicate MRI in particular with echoplanar imaging (EPI) techniques. Therefore, alternative diffusion-weighting pulse sequence types such as single-shot fast-spin-echo sequences or segmented EPI techniques became important alternatives for quantitative DWI of the vertebral bone marrow.

This review first describes pulse sequence types that are particularly important for DWI of the vertebral bone marrow. Then, data from 21 studies that performed diffusion measurements of normal vertebral bone marrow are reviewed; summarizing all results, the apparent diffusion coefficient (ADC) of normal vertebral bone marrow is typically found between 0.2 and $0.6 \times 10^{-3}\,\mathrm{mm}^2/\mathrm{s}$. Finally, DWI of vertebral compression fractures is discussed. Numerous studies demonstrate significantly greater ADCs in osteoporotic fractures (typically between 1.2 and $2.0 \times 10^{-3}\,\mathrm{mm}^2/\mathrm{s}$) than in malignant fractures or lesions (typically 0.7 to $1.3 \times 10^{-3}\,\mathrm{mm}^2/\mathrm{s}$). Alternatively, several studies used the (qualitative) image contrast of diffusion-weighted acquisitions for differentiation of lesion etiology: A very good lesion differentiation can be achieved particularly with diffusion-weighted steady-state free precession sequences, which depict malignant lesions hyperintense relative to normal-appearing vertebral bone marrow in contrast to hypointense or isointense osteoporotic lesions.

## Key words

Diffusion-weighted magnetic resonance imaging; Spinal column; Vertebral bodies; Vertebral bone marrow; Vertebral compression fractures

## Corresponding author

Olaf Dietrich, PhD
Josef Lissner Laboratory for Biomedical Imaging, Institute for Clinical Radiology
Ludwig-Maximilians-University Hospital Munich, Germany
Marchioninistr. 15, 81377 Munich, Germany
Phone: +49 (89) 4400-74622, Fax: +49 (89) 4400-74627
E-mail: od@dtrx.net

## Abbreviations used

ADC: apparent diffusion coefficient, DWI: diffusion-weighted MR imaging, EPI: echo-planar imaging, FSE: fast spin echo, LSDI: line scan diffusion imaging, MRI: magnetic resonance imaging, msEPI: multi-shot echoplanar imaging, rsEPI: readout-segmented echoplanar imaging, ssEPI: single-shot echoplanar imaging, ssFSE: single-shot fast spin echo, SSFP: steady-state free precession, STIR: short-TI inversion recovery

## Introduction

Diffusion-weighted magnetic resonance imaging (DWI) is a well-established technique with numerous important applications in clinical diagnostics of the brain (1–5) and the body (6–13) as well as in research settings (14–18). The defining property of DWI is its sensitivity to the microscopic thermal random motion (the so-called *self-diffusion*) of molecules, e. g., of water molecules in tissue. This thermal motion causes an attenuation of the measured diffusion-weighted MRI signal, which can be evaluated qualitatively, i. e., in terms of image contrast, or quantitatively by calculation of the diffusion coefficient as the physical quantity describing molecular self-diffusion (19–23).

Self-diffusion of water molecules in biological tissues is in general restricted by the microscopic cellular tissue structure, i. e., by cell membranes, by macromolecules in and around the cells, and by cell organelles. The diffusion coefficient of water measured in tissue is therefore always lower than the free diffusion coefficient of pure water. This effective diffusion coefficient is called *apparent diffusion coefficient* (ADC), $D_{\mathrm{app}}$, and is the quantity that is measured in DWI in vivo. It depends on the microscopic geometry of the tissue, but also – in contrast to the diffusion coefficient of pure liquids – on the parameters used for DWI (in particular on the diffusion time $\tau$) (24–26).

The dependence of the ADC on the cellular microstructure makes DWI sensitive to pathological tissue changes associated, e. g., with neoplastic diseases, which frequently exhibit increased local cellular density (cellularity) reflected by decreased ADCs compared to normal tissue. In later disease stages, increasing ADCs may be observed because of necrotic tissue changes. Thus, DWI has been applied for tumor detection, tumor characterization, and for therapy follow-up examinations in virtually all organs of the body (5, 6, 8, 11–13).

In this review, we summarize a large selection of studies published between 1998 and 2015, in which DWI is applied to the bone marrow of the human vertebral bodies. The main focus is on results about DWI of normal vertebral bone marrow (including also data on osteoporotic bone marrow), and on the application of DWI in patients with (benign or malignant) vertebral compression fractures. In the first part of this review article, we will present an overview over the anatomy and tissue composition of the spinal column, followed by a discussion of those diffusion-weighting MRI pulse sequence types that are particularly important for DWI of the vertebrae. Subsequently, numerous measurements of the ADC of normal-appearing vertebral bone marrow are summarized and the influence of different acquisition techniques and imaging parameters is discussed. Finally, diffusion studies of vertebral compression fractures are reviewed, focusing first on ADC measurements to differentiate benign and malignant vertebral lesions. Then, qualitative DWI of vertebral compression fractures is discussed with a special emphasis on the application of diffusion-weighted steady-state free precession (SSFP) techniques.

## Anatomy and tissue composition of the spinal column

The human vertebral column consists of 33 to 34 vertebrae; 24 of these are articulating vertebrae in the cervical, thoracic, and lumbar spine, while typically 9 or 10 fused vertebrae are found in the sacrum and coccyx (27). 23 intervertebral disks lie between the articulating vertebrae (except between the first and second cervical vertebrae). The (articulating) vertebrae are named (in craniocaudal direction) C1 to C7, T1 to T12, and L1 to L5 in the cervical, thoracic, and lumbar spine, respectively.

MRI-visible are predominantly the intervertebral disks (because of their high water content) and – as the main tissue of interest of this article – the bone marrow of the vertebral bodies, i. e., the tissue in the cavities of the trabecular (cancellous) bone.

In contrast to the cortical (compact) bone or the cancellous bone itself with low proton content and extremely short transverse ($T_2$) relaxation times, the bone marrow contains relatively large amounts of both MRI-visible fat and water. Normal bone marrow in the vertebrae consists of red (hematopoietic) marrow – constantly producing the mature blood cells – and yellow marrow containing predominantly fat cells (28). The fraction of yellow bone marrow is increasing with age, i. e., the relative contributions of water and fat to the MRI signal are strongly varying with age. The volume ratio of fatty tissue within the bone marrow is about 15 % in childhood and adolescence and increases to about 45 % in subjects older than 70 years (28).

Important for MRI is also the spongy microstructure of the trabecular bone with its typical pore dimension (trabecular spacing) in the order of 0.5 to 1 mm and a trabecular thickness of about 0.1 to 0.2 mm resulting in bone surface-to-volume ratios of about $10\,\mathrm{mm}^{-1}$ with correspondingly large interface areas between bone marrow and bone (29, 30). Substantial differences of the magnetic susceptibility of trabecular bone on the one hand ($\chi_{\mathrm{bone}} \approx -11 \times 10^{-6}$ in the SI unit system) and of bone marrow on the other hand with $\chi_{\mathrm{water}} = -9.05 \times 10^{-6}$ and $\chi_{\mathrm{fat}} = -8.44 \times 10^{-6}$ (31) result in strong magnetic field gradients within the bone marrow and, thus, drastically shortened $T_2^*$ relaxation times in the order of 8 to 10 ms (32, 33).

The intervertebral disks separate the articulating vertebrae anatomically and visually in MRI; they consist of three major anatomical structures: the outer, ring-shaped anulus fibrosus, the central nucleus pulposus, and the cartilaginous endplates (34). Both the inner ring of the anulus and the nucleus contain substantial amounts of water (but no relevant amounts of fat) and appear therefore bright on $T_2$-weighted or proton-density-weighted MRI.

## Basics of DWI and technical considerations

In DWI of the spinal column, the choice of the optimal diffusion-weighting pulse sequence is both more complicated and still more controversial than in DWI of many other human organs. In particular, the frequently used diffusion-weighting single-shot spin-echo echoplanar imaging (ssEPI)

pulse sequence exhibits certain disadvantages when applied for imaging of the vertebral bone marrow and is, therefore, in many studies replaced by alternative techniques as described below.

The basis of DWI is to increase the sensitivity of the MRI signal to the microscopic thermal random motion of water molecules, which is technically achieved by inserting an additional pair of "diffusion-weighting" gradient pulses into existing pulse sequences (20, 23, 35). These gradients cause an exponential attenuation of the measured signal that depends on the diffusion coefficient as well as on the amplitude, duration, and separation of the gradients. The influence of the gradients is summarized as "diffusion weighting" (or b-value) of the sequence. Quantitatively, the attenuation, i. e., the ratio of measured signal intensity $S(D_{\text{app}}, b)$ and the signal intensity without diffusion sensitizing, $S_0$, is:

$$\frac{S(D_{\text{app}}, b)}{S_0} = \exp(-bD_{\text{app}}). \quad (1)$$

Thus, a measurement of signal attenuations at different b-values enables the estimation of the ADC by fitting Eq. 1 to the measured data points.

The diffusion coefficient $D$ describes the statistical distribution of diffusion distances $\Delta\boldsymbol{x}$ after a diffusion time $\tau$ in terms of the variance $\langle\Delta\boldsymbol{x}^2\rangle = 6D\tau$. In applications in vivo, $D$ is typically expressed in units of $10^{-3}\,\text{mm}^2/\text{s} = \mu\text{m}^2/\text{ms}$. The diffusion coefficient of free water is $D \approx 2.0 \times 10^{-3}\,\text{mm}^2/\text{s}$ at a temperature of 20 °C (room temperature) and $D \approx 3.1 \times 10^{-3}\,\text{mm}^2/\text{s}$ at body temperature (37 °C). The ADC of biological tissues is generally lower than the diffusion coefficient of pure water and ranges approximately between 0.5 and $2.5 \times 10^{-3}\,\text{mm}^2/\text{s}$.

Many different pulse sequence types can be extended by diffusion gradients to acquire diffusion-weighted image data, and numerous review articles are available that describe in detail sequence techniques available for DWI of the vertebral bone marrow and other structures outside the brain (13, 36–38). The first MR imaging pulse sequences extended by diffusion gradient pulses were (in the mid-1980s) spin-echo (SE) and stimulated-echo (STE) pulse sequences (21, 22, 39). Since these sequences are very slow and – when used for DWI – extremely sensitive to motion, they are rarely used for DWI in humans today. A promising modification of the SE approach is line scan diffusion imaging (LSDI); by exciting one-dimensional "lines" instead of the usual two-dimensional imaging plane, the repetition time can be substantially shortened and the final image can be reconstructed from magnitude data, which reduces the sensitivity to motion and to susceptibility variations (40, 41).

Today, the majority of clinical DWI examinations are performed with diffusion-weighting single-shot spin-echo echo-planar imaging sequences (42, 43), which allow the very fast and motion-insensitive acquisition of DWI data – however, with only limited spatial resolution (typically $128 \times 128$ pixels) and increased sensitivity to magnetic field inhomogeneities and eddy currents. These limitations are generally tolerated in DWI applications of the brain, where relatively small fields of view and good field shimming are feasible. In other body areas, in particular in the lungs or around the neck and the spine, diffusion-weighted ssEPI acquisitions with acceptable image quality remain difficult, because strong local variations of magnetic susceptibility cause dephasing and signal loss in all gradient-echo-based acquisition techniques. In addition, macroscopic magnetic field inhomogeneities at tissue-air or soft-tissue-bone interfaces result in severe geometric distortions of EPI acquisitions. Only in recent years, the image quality of diffusion-weighted ssEPI in the body improved substantially after the introduction of better gradient hardware with reduced eddy currents and with further optimization of the ssEPI pulse sequences such as parallel-imaging acceleration (44–47) or dynamic slice-dependent shimming (48).

An alternative to single-shot EPI measurements with increased robustness in the presence of severe field inhomogeneities is the so-called segmented or "multi-shot" EPI (msEPI) sequence. The msEPI sequences either acquire every $n$-th line in k-space dividing the image acquisition in $n$ separate excitations (49, 50), or they acquire only a small strip of k-space data in readout direction after each excitation (readout-segmented EPI, rsEPI) (51, 52). Both approaches are substantially slower than conventional single-shot EPI sequences and they are more sensitive to motion requiring motion-correction algorithms for satisfying image quality.

Another class of diffusion-weighting pulse sequences is based on fast-spin-echo (FSE) or turbo-spin-echo sequences, i. e., on pulse sequences that acquire a train of spin echoes after each excitation. Using spin echoes instead of gradient echoes, these sequences are much more robust than ssEPI techniques in the presence of strong susceptibility variations (53, 54). In particular diffusion-weighting single-shot FSE (ssFSE) sequences have been successfully employed for DWI of the spinal column. Similar to ssEPI sequences, the maximum matrix size is typically limited to about $128 \times 128$ pixels because of the decay of the transverse magnetization with the relaxation time $T_2$.

Finally, steady-state free precession (SSFP) sequences – also known as contrast-enhanced Fourier-acquired steady-state technique (CE-FAST) (55) or reversed fast imaging with steady precession (PSIF) sequences (56) – can be extended by a diffusion-gradient pulse. In contrast to all other diffusion-weighting pulse sequences described above, only a single (i. e., unpaired) gradient pulse is inserted into the SSFP sequence (57, 58). Since each radio-frequency pulse acts simultaneously also as excitation and refocusing (spin-echo-generating) pulse, the dephasing of the diffusion gradient is rephased in the (immediate) subsequent or a later repetition of the basic pulse series. Consequently, the time interval between dephasing and rephasing diffusion gradient pulses is not uniquely defined and the quantification of the diffusion weighting is very difficult, since it depends not only on the diffusion gradient pulses themselves (with duration $\delta$ and amplitude $G$), but also on the relaxation times, $T_1$ and $T_2$, of the tissue as well as on the flip angle $\alpha$, the echo time $T_E$, and the repetition time $T_R$ of the pulse sequence (59, 60). The diffusion-weighted signal $S_\perp^-$ of the SSFP sequence relative to the fully relaxed magnetization $M_0$ is given by

$$\frac{S_\perp^-}{M_0} = -\frac{(1-E_1)\,E_2 A_2^{1/3}\left(F_1 - E_2 A_1 A_2^{-2/3}\right)\sin(\alpha)}{r - F_1 s}, \quad (2)$$

with

$$F_1 = K - \sqrt{K^2 - A_2^{-2}},$$

$$K = \frac{1 - E_1 A_1 \cos(\alpha) - E_2^2 A_1^2 A_2^{2/3}(E_1 A_1 - \cos(\alpha))}{E_2 A_1 A_2^{4/3}(\cos(\alpha) + 1)(1 - E_1 A_1)},$$

$$r = 1 - E_1 \cos(\alpha) + E_2^2 A_1 A_2^{-1/3}(\cos(\alpha) - E_1),$$

$$s = E_2 A_1 A_2^{4/3}(1 - E_1 \cos(\alpha)) + E_2 A_2^{1/3}(\cos(\alpha) - E_1),$$

$$A_1 = \exp(-(\gamma G \delta)^2 T_R \cdot D), \quad A_2 = \exp(-(\gamma G \delta)^2 \delta \cdot D),$$

$$E_1 = \exp(-T_R/T_1), \quad E_2 = \exp(-T_R/T_2),$$

where the influence of the diffusion coefficient $D$ is described by the two attenuation factors $A_1$ and $A_2$. In general, it is not easily possible to estimate the diffusion coefficient based on the measured signals $S_\perp^-$ of the DW-SSFP sequence. Nevertheless, this sequence has been applied very successfully for qualitative DWI of the vertebral bone marrow, and in particular for the differentiation of benign and malignant vertebral compression fractures as is described below.

## ADCs of normal-appearing vertebral bone marrow

Numerous studies published between 2000 and 2014 provided reference ADCs of normal (or normal-appearing) vertebral bone marrow. The main results of these studies are summarized in Fig. 1 and in Table 1 together with the pulse sequence type and the b-values used for the measurement. If the authors of a study did not provide a single mean value and standard deviation, results, e. g., from different vertebrae were statistically combined; in two cases (61, 62), median and quartile values were used to estimate the mean and the standard deviation (63). A typical example of DWI in the lumbar spine of a healthy volunteer using a fat-saturated ssFSE sequence is shown in Fig. 2.

The majority of the listed studies found ADCs of normal vertebral bone marrow in a range between 0.2 and $0.6 \times 10^{-3}\,\mathrm{mm^2/s}$. This is a relatively low ADC compared to almost all other tissues (except fat tissue) in the human body with typical ADCs between 0.7 (e. g., in white matter) and $2.4 \times 10^{-3}\,\mathrm{mm^2/s}$ (e. g., in the kidneys). The comparably large variations of the presented results (by several 100 % even after discarding the most obvious outliers) may be explained by experimental differences including different pulse sequences and varying diffusion weightings. In particular, many relatively low ADCs ($< 0.4 \times 10^{-3}\,\mathrm{mm^2/s}$) were acquired with sequences without fat saturation (such as ssFSE sequences) and may be influenced by the contribution of the fat signal to the measured signal intensities. In contrast to EPI sequences, for which fat-saturation pulses are mandatory to avoid severe chemical shift artifacts, ssFSE sequences can be used with and without fat suppression. If used without fat suppression, the diffusion-weighted signal is the sum of the diffusion-attenuated water signal and the – for different diffusion weightings almost constant – fat signal; the calculated ADC appears reduced, since the signal is less attenuated at increasing b-values than the water signal alone (82). This is nicely illustrated in data from the study by Oner et al. (74), in which ssFSE acquisitions without fat-signal suppression and ssEPI acquisitions with fat saturation are directly compared.

The selection of b-values can influence the measured ADCs as well. On the one hand, large b-values (greater than $600\,\mathrm{s/mm^2}$) could be regarded as desirable because of the low ADCs, which require a certain b-value range for a precise measurement with sufficient diffusion-induced signal attenuation. On the other hand (and more relevant in practice), large b-values require relatively long echo times and result in low signal intensities, i. e., in data with disadvantageously low signal-to-noise ratio. If the (magnitude) signal at high b-values is dominated by noise, the calculated ADCs are decreased (83). Another effect to be considered for the selection of b-values is that the signal at very low b-values (lower than $100\,\mathrm{mm^2/s}$) may be influenced by perfusion effects, resulting in higher ADCs as discussed below. Several studies preferred therefore an intermediate range of diffusion weightings between 50 and $600\,\mathrm{s/mm^2}$ (cf. Table 1).

A few studies examined systematic variations of the ADC of vertebral bone marrow depending on the location of the vertebrae and on the age of the subjects. A trend to decreasing ADCs from L1 to L5 was found by Eguchi et al. (78) and by Hillengass et al. (61). Similarly, a higher ADC for T10 than for L3 was found by Dutoit et al. (81); these results are summarized in Table 2. A slow decrease of the ADC with age was observed by Yeung et al. (70) and by Herrmann et al. (80); estimated from the data presented in these two publications, the annual decrease of ADC is about $-0.0014 \times 10^{-3}\,\mathrm{mm^2/s/year}$ and $-0.0015 \times 10^{-3}\,\mathrm{mm^2/s/year}$, respectively (i. e., the ADC is decreased by about $0.1 \times 10^{-3}\,\mathrm{mm^2/s}$ over a period of 70 years). In contrast to these results, no such correlation of ADC and age was found by Hillengass et al. (61) and by Zhang et al. (84).

A slight decrease of the ADC with increasing degrees of osteoporosis (i. e., with decreasing bone mineral density and increasing fat fraction) was observed by Yeung et al. (70), Griffith et al. (72), Hatipoglu et al. (73), and Tang et al. (77) as summarized in Table 3; in contrast, Ueda et al. (85) observed a slight *increase* of the ADC in subjects with lower bone marrow density, which is explained by the authors as being caused by generally higher bone marrow densities (i. e., by a differently selected patient cohort) than in other studies.

Several studies discuss the influence of non-monoexponential diffusion in bone marrow or of intravoxel incoherent motion (IVIM) effects. In 2003, Bammer et al. demonstrated bi-exponential diffusion behavior of bone marrow over a b-value range from 5 to $3005\,\mathrm{s/mm^2}$ with a fast diffusion component (relative fraction about 10 %) of about $1.5 \times 10^{-3}\,\mathrm{mm^2/s}$ and a slow component of $0.07 \times 10^{-3}\,\mathrm{mm^2/s}$ (69). This measurement at very high b-values does not refer to (perfusion-related) IVIM effects as they are understood today and neither the slow nor the fast component agrees with the average ADC of $0.2 \times 10^{-3}\,\mathrm{mm^2/s}$ measured for b-values of 5 and $650\,\mathrm{s/mm^2}$ in the same study.

Classical IVIM measurements in vertebral bone marrow were first performed by Yeung et al. in 2004, who demonstrated graphically a substantial perfusion component at low b-values $< 100\,\mathrm{s/mm^2}$, which was, however, not quantified in this study (70). Consequently, the authors recom-

Table 1: Apparent diffusion coefficients of normal vertebral bone marrow

| Study (reference) | sequence* | b-values† (s/mm$^2$) | fat sat. | $n$‡ | ADC ($10^{-3}$ mm$^2$/s) |
|---|---|---|---|---|---|
| Herneth et al. 2000 (64) | msEPI | 0, 440, 880 | yes | 5 | 1.13±0.23 |
| Dietrich et al. 2001 (65) | radSE | 50...500 (4) | no | 36 | 0.33±0.05 |
| Chan et al. 2002 (66) | ssEPI | 200...1000 (4) | yes | 32 | 0.23±0.05 |
| Byun et al. 2002 (67) | ssSTE | 0, 650 | no | 3 | 0.33±0.03 |
| Herneth et al. 2002 (68) | msEPI | 440, 880 | yes | 22 | 1.66±0.38 |
| Bammer et al. 2003 (69) | LSDI | 5, 650 | no | 15 | 0.23±0.08 |
| Yeung et al. 2004 (70) | ssEPI | 0...500 (10) | yes | 20 | 0.50±0.09 |
| Pui et al. 2005 (71) | ssEPI | 0, 500, 1000 | yes | 103 | 0.36±0.21 |
| Griffith et al. 2006 (72) | ssEPI | 0...500 (6) | yes | 18 | 0.46±0.08 |
| Hatipoglu et al. 2007 (73) | ssEPI | 0, 600 | yes | 68 | 0.46±0.03 |
| Oner et al. 2007 (74) | ssEPI | 0, 600 | yes | 24 | 0.53±0.15 |
| | ssFSE | 0, 600 | no | 24 | 0.35±0.15 |
| Raya et al. 2007 (75) | ssFSE | 50...750 (4) | no | 20 | 0.21±0.06 |
| Byun et al. 2007 (76) | ssSTE | 0, 650 | no | 7 | 0.21±0.06 |
| Tang et al. 2010 (77) | ssEPI | 0, 300 | yes | 24 | 0.47±0.03 |
| Hillengass et al. 2011 (61) | ssFSE | 0, 400 | no | 148 | 0.42±0.07 |
| Eguchi et al. 2011 (78) | ssEPI | 0, 1000 | yes | 75 | 0.46±0.12 |
| Biffar et al. 2011 (32) | ssFSE | 100...600 (4) | yes | 40 | 0.58±0.16 |
| Pozzi et al. 2012 (79) | ssEPI | 0, 800 | yes | 33 | 0.41±0.23 |
| Herrmann et al. 2012 (80) | ssEPI | 50, 400, 800 | yes | 88 | 0.50±0.08 |
| Sung et al. 2014 (62) | ssEPI | 0, 800 | yes | 55 | 0.42±0.14 |
| Dutoit et al. 2014 (81) | ssEPI | 0,1000 | yes | 11 | 0.37±0.33 |
| **typical range** | | **0...600** | | | **0.2...0.6** |
| **averaged values** | | | | **871** | **0.454±0.258** |

*radSE: radial spin-echo sequence, ssSTE: single-shot stimulated echo sequence
†if more than 3 b-values were used, the range is provided with the number of b-values in parentheses
‡number of evaluated vertebrae

Table 2: Dependence of the ADC of vertebral bone marrow on anatomical location

| Study (reference) | sequence | b-values (s/mm$^2$) | $n$* | ADC ($10^{-3}$ mm$^2$/s) L1 (T10†) | L2 | L3 | L4 | L5 |
|---|---|---|---|---|---|---|---|---|
| Hillengass et al. 2011 (61) | ssFSE | 0, 400 | 30 | 0.46±0.37 | 0.43±0.32 | 0.42±0.28 | 0.40±0.30 | 0.43±0.24 |
| Eguchi et al. 2011 (78) | ssEPI | 0, 1000 | 15 | 0.50±0.10 | 0.48±0.11 | 0.49±0.12 | 0.43±0.13 | 0.38±0.12 |
| Dutoit et al. 2014 (81) | ssEPI | 0, 1000 | 11 | 0.45±0.42 | — | 0.29±0.20 | — | — |

*number of subjects
†T10 in study by Dutoit et al.

Table 3: Dependence of the ADC on the vertebral bone marrow density

| Study (reference) | sequence | b-values* (s/mm$^2$) | ADC ($10^{-3}$ mm$^2$/s) ($n$†) normal | osteopenia | osteoporosis |
|---|---|---|---|---|---|
| Yeung et al. 2004 (70) | ssEPI | 0...500 (10) | 0.44±0.11 (13) | 0.42±0.14 (12) | 0.42±0.12 (10) |
| Griffith et al. 2006 (72) | ssEPI | 0...500 (6) | 0.46±0.08 (18) | 0.41±0.12 (30) | 0.43±0.12 (55) |
| Hatipoglu et al. 2007 (73) | ssEPI | 0, 600 | 0.46±0.03 (68) | 0.42±0.03 (70) | 0.38±0.02 (66) |
| Tang et al. 2010 (77) | ssEPI | 0, 300 | 0.47±0.03 (24) | 0.41±0.02 (25) | 0.39±0.02 (29) |

*if more than 3 b-values were used, the range is provided with the number of b-values in parentheses
† number of evaluated vertebrae

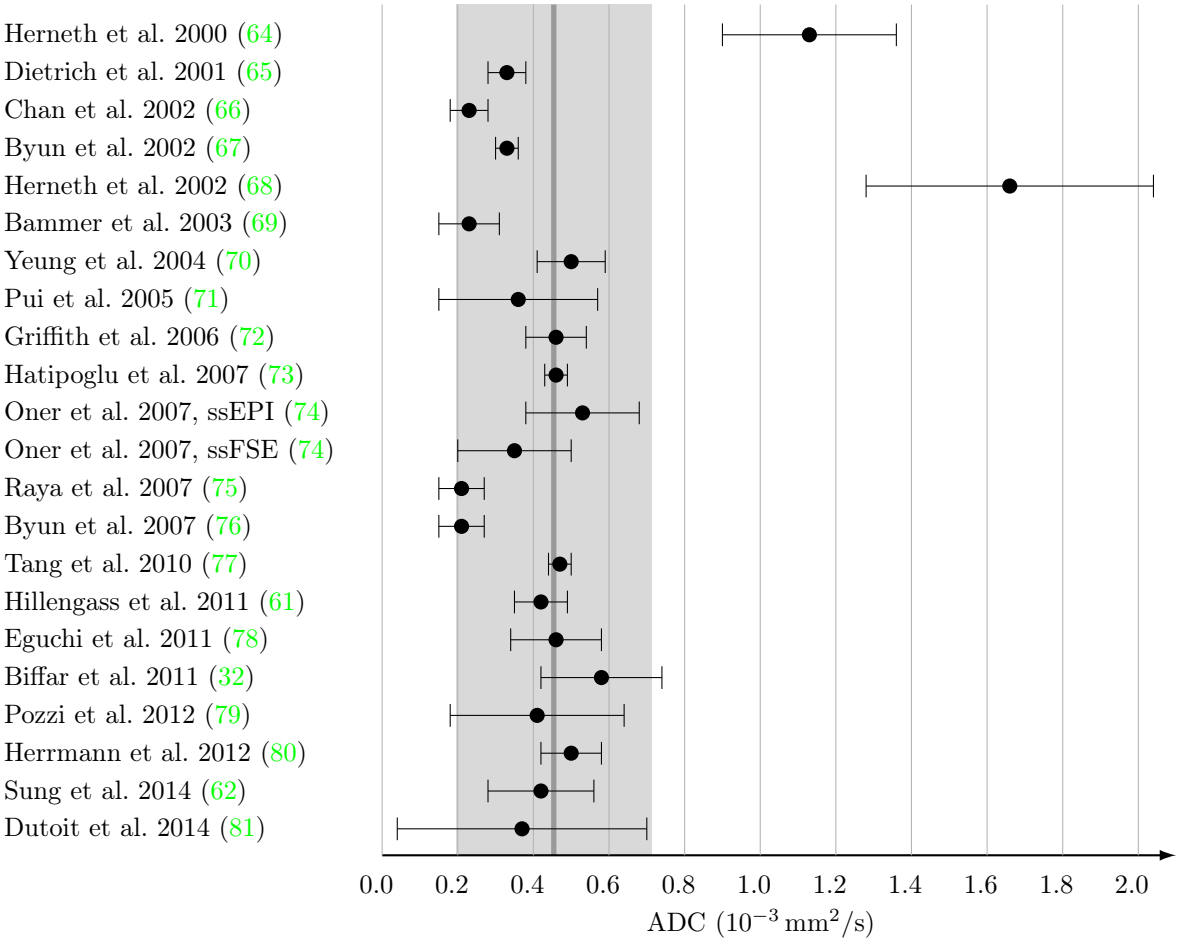


Figure 1: Apparent diffusion coefficients of normal vertebral bone marrow from the studies listed in Table 1. The shaded area with the thicker vertical line is the averaged value with standard deviation over all listed studies.

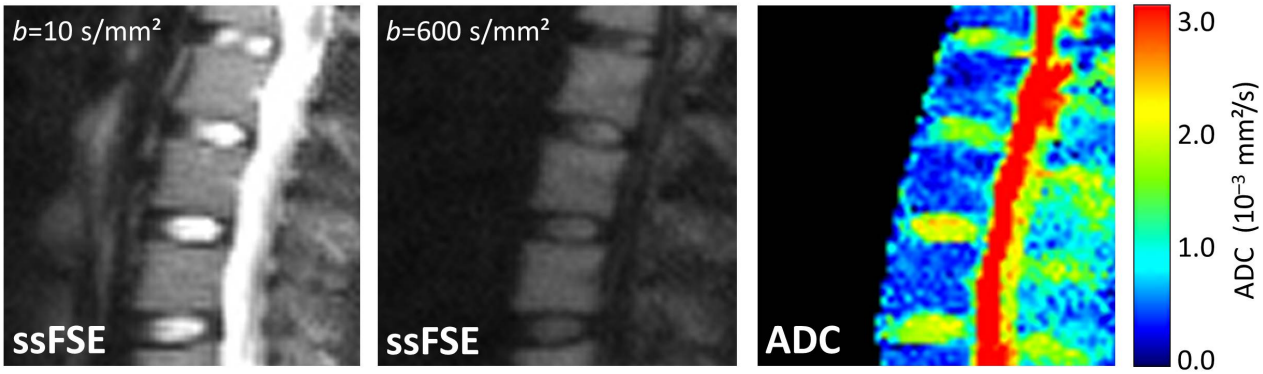


Figure 2: Diffusion-weighted images (acquired with a fat-saturated ssFSE sequence) and ADC map of the lumbar spine of a 35-year-old female healthy volunteer. The average ADC of the vertebral bone marrow is $(0.66 \pm 0.17) \times 10^{-3}$ mm$^2$/s; the average ADC of the intervertebral disks is $(1.62 \pm 0.39) \times 10^{-3}$ mm$^2$/s.

mended to use minimum b-values greater than 0 to reduce the influence of perfusion on the determined diffusion coefficients, which was implemented, e. g., in the studies by Griffith et al. (72), Raya et al. (75), Biffar et al. (32), or Herrmann et al. (80). The results by Dutoit et al. (81) illustrate as well lower diffusion coefficients for 3 b-values 200, 400, and 600 s/mm$^2$ (e. g., $(0.305 \pm 0.058) \times 10^{-3}$ mm$^2$/s for L3) than measured with the b-values 0 and 400 s/mm$^2$ ($(0.439 \pm 0.102) \times 10^{-3}$ mm$^2$/s), which may be explained by the influence of perfusion effects.

A detailed IVIM study in vertebral bone marrow was published by Marchand et al. in 2014 (86) comparing a conventional non-linear bi-exponential fitting approach and a non-negative least-squares (NNLS) approach, which allowed for an arbitrary number of diffusion components. Both approaches gave results compatible with two distinct diffusion components. The conventional bi-exponential analysis resulted in a slow diffusion coefficient of $(0.45 \pm 0.27) \times 10^{-3}$ mm$^2$/s (in good agreement with the ADCs determined in other studies), a fast diffusion coefficient, $D^*$, of $(63.0 \pm 14.5) \times 10^{-3}$ mm$^2$/s, and a perfusion fraction of 27 %. A recently published IVIM study by Ohno et al. finds substantially lower values of $D^*$ in vertebral bone marrow between about 3 and $8 \times 10^{-3}$ mm$^2$/s, a perfusion fraction between 10 and 20 %, and a slow (normal) diffusion coefficient between 0.1 and $0.3 \times 10^{-3}$ mm$^2$/s (87). Further research is required to confidently estimate typical ranges of IVIM parameters in normal vertebral bone marrow.

For comparison and to conclude this section about quantitative diffusion measurements in normal vertebral bone marrow, the ADC of normal intervertebral disks is considered as reference tissue in the immediate neighborhood of the vertebrae: The ADC of normal intervertebral disks has been described in a range between about 1.5 (e. g., 65, 69, 88, 89) and $2.0 \times 10^{-3}$ mm$^2$/s (e. g., 75, 90–92), i. e., significantly higher than the ADC of normal vertebral bone marrow (cf. Fig. 2).

## ADCs of vertebral compression fractures and metastases

A very important diagnostic question in MRI of the spinal column, which is notoriously difficult to answer with conventional MRI sequences, is the differentiation of benign and malignant vertebral compression fractures, i. e., of fractures caused either by osteoporosis or by neoplastic bone-marrow lesions, respectively. Both lesion types appear frequently hypointense in $T_1$-weighted MRI and hyperintense in short-TI inversion recovery (STIR) MRI (93); and they are both predominantly found in elderly patients. These contrast properties are illustrated in Figs. 3 and 4.

In contrast to conventional MR image contrast (i. e., $T_1$ weighting or STIR), DWI was demonstrated in numerous studies to be a valuable tool for the differentiation of vertebral compression fractures. One important approach chosen in these studies is to evaluate the ADC of the vertebral lesion as a means for differentiation based on the observation that the ADC of benign, osteoporotic fractures is generally higher than the ADC of metastatic lesions or malignant fractures caused by tumor infiltration. The ADCs found by several studies are summarized in Table 4 and in Fig. 5.

The ADC of both kinds of lesions is significantly higher than the ADC of normal vertebral bone marrow shown in Table 1. (Only a single early study by Zhou et al. reports untypically low ADCs for both types of lesions (94).) The results in Table 4 for malignant lesions comprise both vertebral compression fractures caused by tumor infiltration or bone metastases and the ADCs of unfractured vertebrae with neoplastic lesions, because these two types of pathologies were not strictly separated in several studies. Typical ADCs for these malignant lesions are in the range from about 0.7 to $1.3 \times 10^{-3}$ mm$^2$/s; the mean value calculated from all individual studies is $(0.933 \pm 0.367) \times 10^{-3}$ mm$^2$/s. In contrast, typical ADCs of osteoporotic fractures are in the range from about 1.2 to $2.0 \times 10^{-3}$ mm$^2$/s with a mean value of $(1.681 \pm 0.531) \times 10^{-3}$ mm$^2$/s. Only a single study reported a lower ADC for osteoporotic fractures than for malignant lesions without any explanation for this disagreeing result (79). Exemplary diffusion-weighted images of vertebral bone marrow and lesions are shown in Figs. 6 and 7.

It is not yet fully understood which pathophysiological properties contribute to the described ADC differences of vertebral lesions. A plausible hypothesis is that the ADC in osteoporotic fractures is increased because of the presence of bone marrow edema (i. e., the greater amount of free water) and the disruption of the trabecular structure. In malignant lesions, on the other hand, the molecular diffusion is assumed to be restricted by the higher cellular density of tumor tissue resulting in lower ADCs (93).

Most studies describe a certain overlap of the ADCs associated with osteoporotic or malignant lesions, i. e., the lesions cannot be completely separated based on the ADC alone. By defining an ADC threshold, a successful classification is, however, possible in many cases; the statistical performance of such a classification can be described by the sensitivity and specificity of the differentiation. Quantitative evaluations of the sensitivity and specificity are given by Wonglaksanapimon et al. (101), Taşkın et al. (99), Sung et al. (62), and Geith et al. (100); the results of these studies are summarized in Table 5. The reported sensitivities range from 85 % to 97 % and the specificities are between 85 % and 100 %. Summarizing, a good to excellent differentiation of benign and malignant vertebral lesions based on the ADC is possible (102).

Four of the studies listed in Table 4 included also inflammatory vertebral lesions such as lesions caused by spondylitis or tuberculosis; the ADC of these lesions was typically between the ADC of osteoporotic and neoplastic lesions with a mean value of $(1.200 \pm 0.409) \times 10^{-3}$ mm$^2$/s. Only few studies evaluated the ADC in other vertebral bone marrow pathologies, e. g., in bone marrow with active myeloma and in remission (103) or in marrow infiltration in children with Gaucher's disease, which showed lower ADCs than bone marrow of healthy controls (104).

## Image contrast in DWI of vertebral compression fractures

Already in 1998, i. e., before the first publications of quantitative ADC measurements in vertebral bone marrow, Baur et al. described the application of a purely qualitatively diffusion-weighting SSFP sequence for the accurate differ-

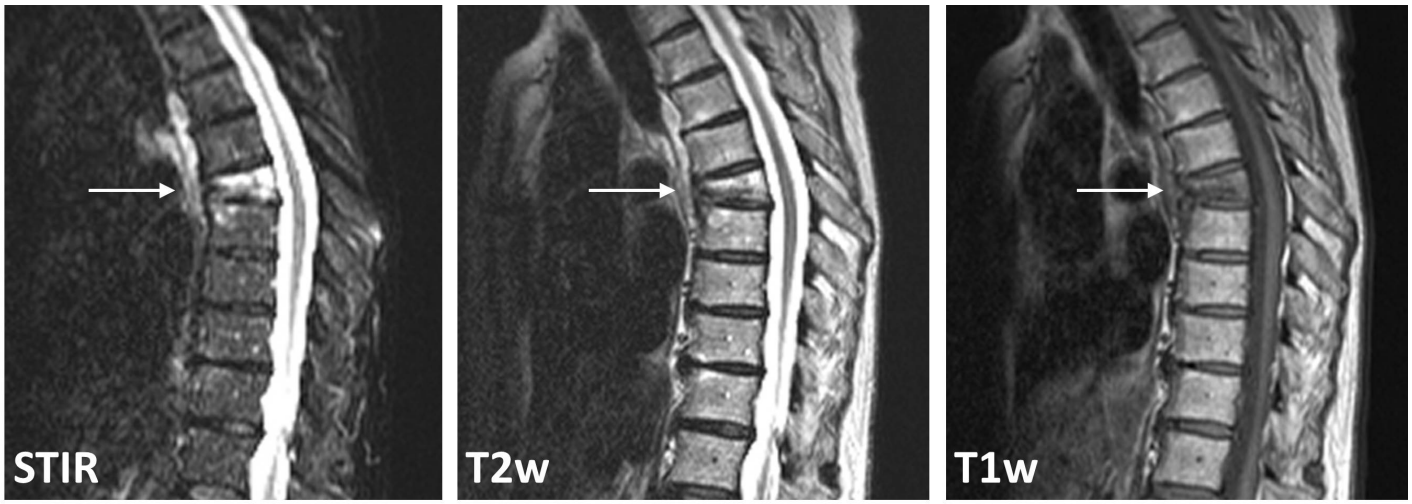


Figure 3: 69-year-old female patient with osteoporotic vertebral compression fracture of T7. The fracture (arrow) is hyperintense on the STIR image, heterogeneous on the $T_2$-weighted image, and hypointense on the $T_1$-weighted image.

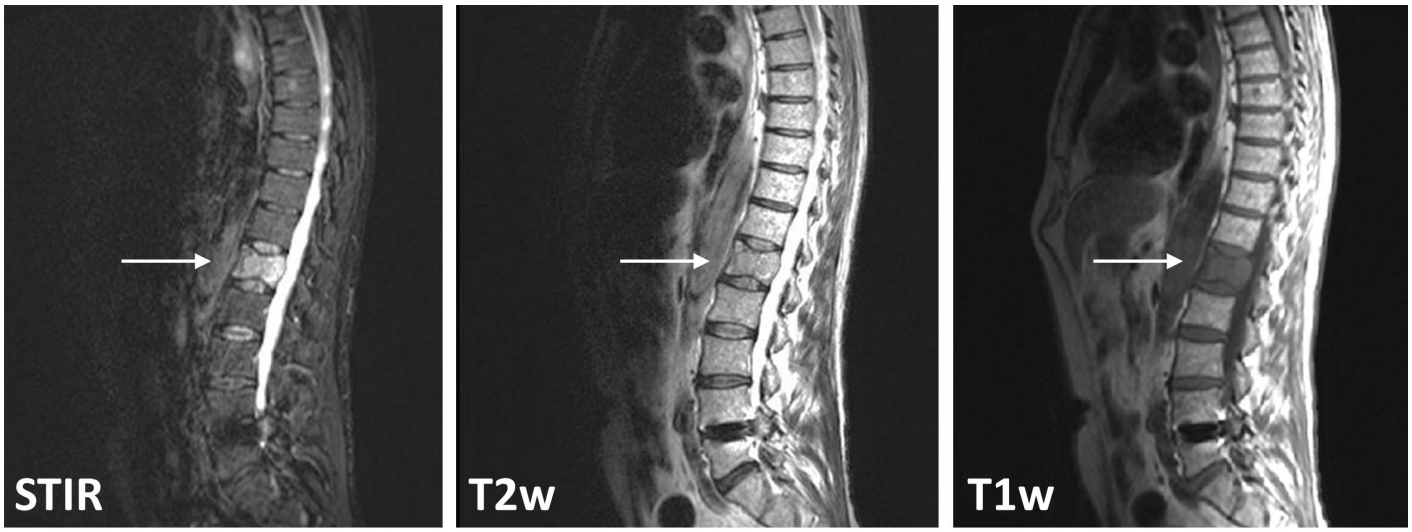


Figure 4: 65-year-old male patient with metastatic vertebral bone-marrow lesion (adenocarcinoma) of L1. The fracture (arrow) is hyperintense on the STIR image, isointense on the $T_2$-weighted image, and hypointense on the $T_1$-weighted image.

Table 4: Apparent diffusion coefficients of vertebral lesions and fractures

| Study (reference) | sequence | b-values* | ADC ($10^{-3}$ mm$^2$/s) ($n^\dagger$) | | |
|---|---|---|---|---|---|
| | | (s/mm$^2$) | osteoporotic fracture | malignant lesions | inflammation |
| Zhou et al. 2002 (94) | ssFSE | 0, 150, 250 | 0.32±0.05 (12) | 0.19±0.03 (15) | — |
| Chan et al. 2002 (66) | ssEPI | 200...1000 (4) | 1.94±0.35 (25) | 0.82±0.20 (18) | 0.98±0.21 (6) |
| Herneth et al. 2002 (68) | msEPI | 440, 880 | 1.61±0.37 (7) | 0.69±0.24 (31) | — |
| Maeda et al. 2003 (95) | LSDI | 5, 1000 | 1.21±0.17 (20) | 0.85±0.18 (63) | — |
| Pui et al. 2005 (71) | ssEPI | 0, 500, 1000 | — | 1.02±0.36 (50) | 1.16±0.40 (78) |
| Tang et al. 2007 (96) | ssFSE | 0, 300 | 2.23±0.21 (18) | 1.04±0.03 (27) | — |
| Balliu et al. 2009 (97) | msEPI | 0, 500 | 1.90±0.39 (15) | 0.92±0.13 (15) | 0.96±0.49 (14) |
| Biffar et al. 2011 (32) | ssFSE | 100...600 (4) | 1.77±0.36 (20) | 1.36±0.39 (20) | — |
| Pozzi et al. 2012 (79) | ssEPI | 0, 800 | 0.65±0.36 (10) | 1.24±0.41 (23) | — |
| Rumpel et al. 2013 (98) | rsEPI | 0, 650 | 1.84±0.37 (34) | 1.22±0.14 (12) | — |
| Taşkın et al. 2013 (99) | ssEPI | 0, 500 | 1.75±0.30 (27) | 0.81±0.32 (74) | 1.54±0.15 (23) |
| Sung et al. 2014 (62) | ssEPI | 0, 800 | 1.83±0.20 (32) | 0.95±0.17 (23) | — |
| Geith et al. 2014 (100) | ssFSE | 100, 250, 400 | 1.80±0.33 (26) | 1.36±0.43 (20) | — |
| **typical range** | | **0...600** | **1.2...2.0** | **0.7...1.3** | **1.0...1.5** |
| **averaged values** | | | **1.681±0.531 (246)** | **0.933±0.367 (391)** | **1.200±0.409 (121)** |

*if more than 3 b-values were used, the range is provided with the number of b-values in parentheses
† number of evaluated vertebrae

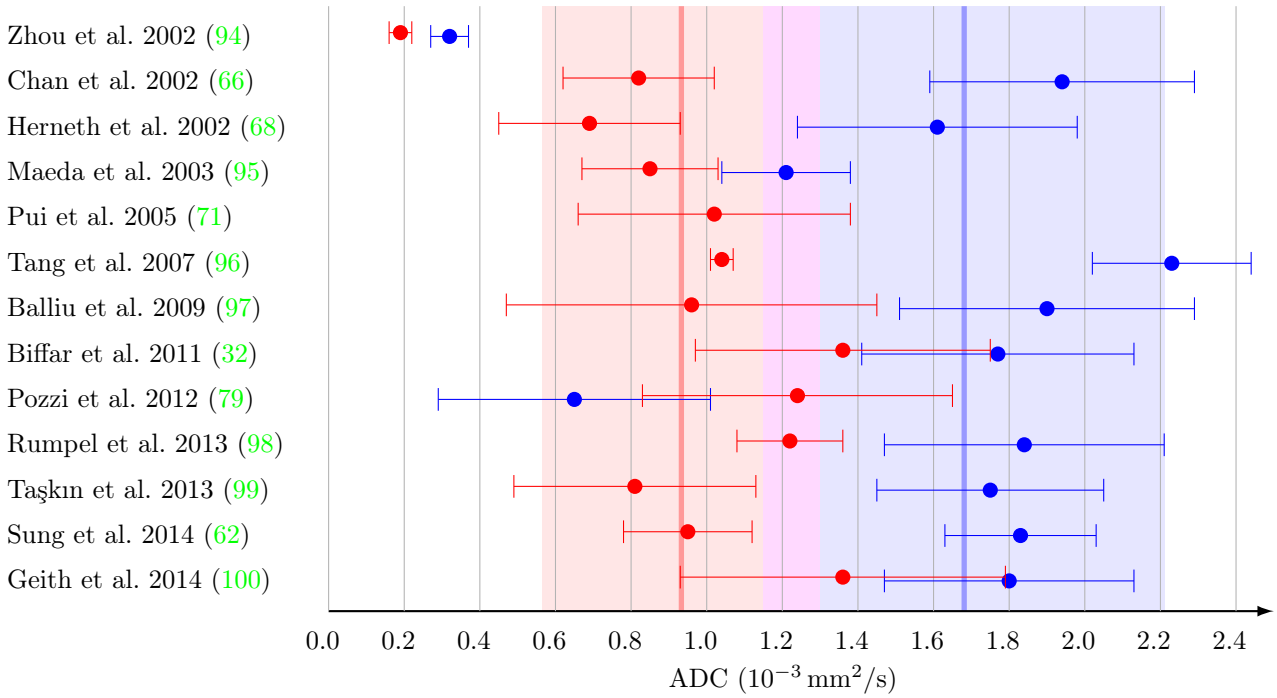


Figure 5: Apparent diffusion coefficients of vertebral bone marrow lesions listed in Table 4; the ADC ranges of malignant lesions or fractures are displayed in red, benign osteoporotic fractures are displayed in blue. The shaded areas with the thicker vertical line are the averaged values with standard deviations over all listed studies; the shaded area in purple denotes the overlap of the standard deviations.

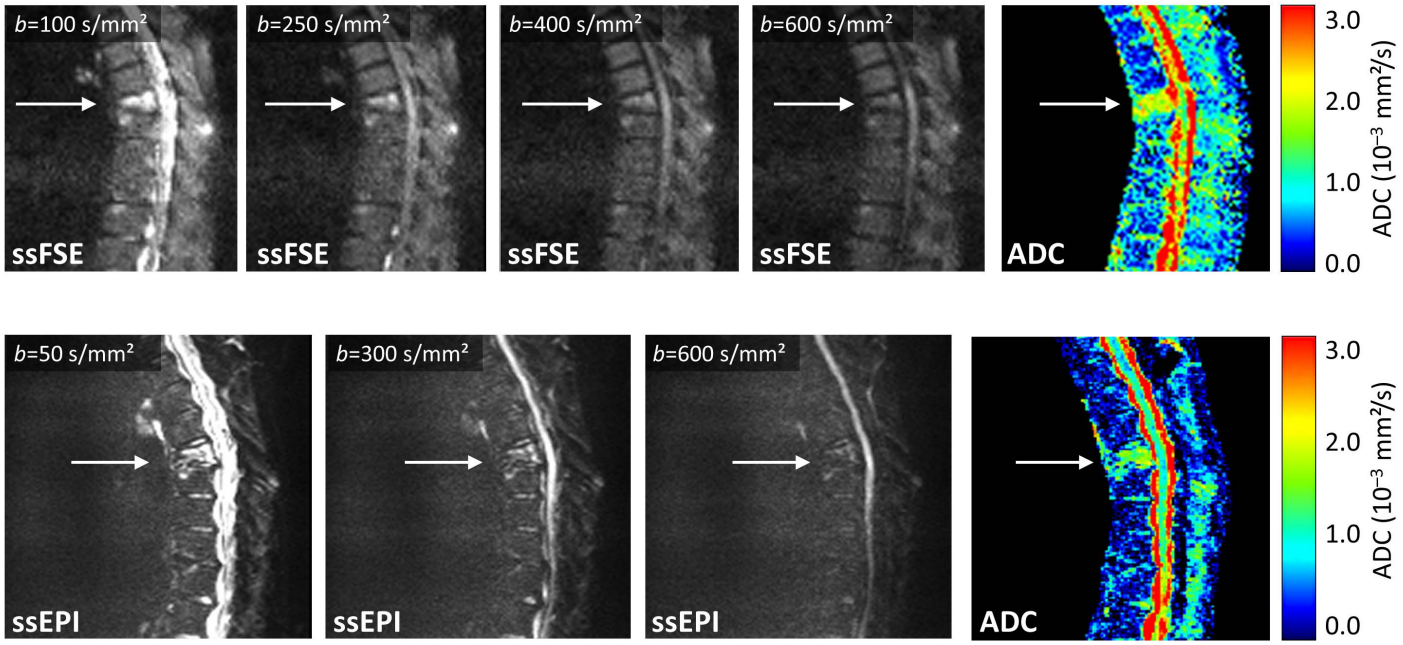


Figure 6: 69-year-old female patient with osteoporotic vertebral compression fracture of T7 (same patient as in Fig. 3). The fracture is hyperintense at low diffusion weightings (b-values) and has approximately isointense contrast (with some signal heterogeneity) at high b-values. The ADC of the fractured vertebra is substantially higher ($2.07 \times 10^{-3}$ mm$^2$/s in ssFSE acquisition, $1.55 \times 10^{-3}$ mm$^2$/s in ssEPI acquisition) than the ADC of the adjacent normal appearing bone marrow (e. g., in T5, $0.54 \times 10^{-3}$ mm$^2$/s in ssFSE acquisition, $0.39 \times 10^{-3}$ mm$^2$/s in ssEPI acquisition). Note the geometric distortion of the spinal canal in the ssEPI acquisitions.

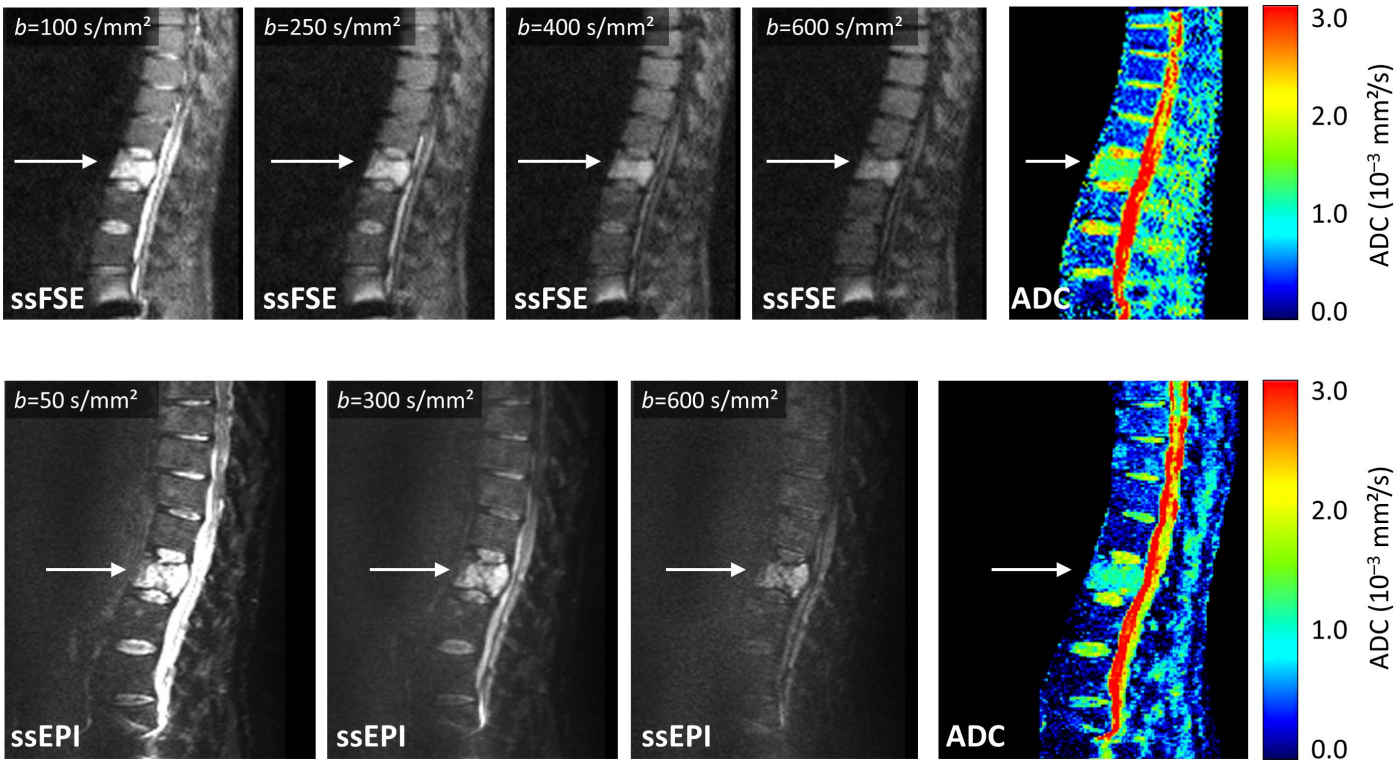


Figure 7: 65-year-old male patient with metastatic vertebral bone-marrow lesion of L1 (same patient as in Fig. 4). The fracture is hyperintense at all applied diffusion weightings. The ADC of the lesion is visibly higher ($1.37 \times 10^{-3}\,\mathrm{mm}^2/\mathrm{s}$ in ssFSE acquisition, $1.20 \times 10^{-3}\,\mathrm{mm}^2/\mathrm{s}$ in ssEPI acquisition) than the ADC of the adjacent normal appearing bone marrow (e. g., in T11, $0.62 \times 10^{-3}\,\mathrm{mm}^2/\mathrm{s}$ in ssFSE acquisition, $0.49 \times 10^{-3}\,\mathrm{mm}^2/\mathrm{s}$ in ssEPI acquisition).

Table 5: Diagnostic performance of ADC to discriminate malignant vertebral lesions

| Study (reference) | $n^*$ | ADC threshold ($10^{-3}\,\mathrm{mm}^2/\mathrm{s}$) | sensitivity (%) | specificity (%) | accuracy (%) |
|---|---|---|---|---|---|
| Wonglaksanapimon et al. 2012 (101) | 39 | $< 0.89$ | 85.7 | 90.6 | 89.7 |
| Taşkın et al. 2013 (99) | 133 | $< 1.32$ | 96.5 | 95.2 | — |
| Sung et al. 2014 ($b = 0, 800\,\mathrm{s/mm}^2$) (62) | 55 | $< 1.242$ | 97 | 100 | 98 |
| Geith et al. 2014 ($b = 100, 250, 400\,\mathrm{s/mm}^2$) (100) | 46 | $< 1.70$ | 85.0 | 84.6 | — |

*number of evaluated lesions

entiation of benign and malignant vertebral lesions based on the visual image contrast (93): In diffusion-weighted SSFP images of the spine, malignant lesions appear predominantly hyperintense while benign lesions are predominantly hypointense or isointense relative to normal vertebral bone marrow as illustrated in Fig. 8. These results were corroborated by several subsequent clinical studies (105–109). The sensitivities for differentiating benign and malignant lesions with diffusion-weighting SSFP sequences are reported between 85 % and 100 %; the specificities between 89 % and 95 % (32, 106, 108, 109). Only a few studies reported disagreeing results with hypointense signal of malignant vertebral lesions (110, 111), which may be explained either by lesions irradiated before imaging or by sclerotic metastases (in this case of prostate tumor) with very low water content.

As a clinically relevant alternative to bone-marrow lesion differentiation based on the ADC, visual differentiation has been frequently discussed since 1998 and numerous studies analyzed the image contrast within a single diffusion-weighted image acquired either with diffusion-weighting SSFP sequences or with other diffusion-weighting techniques such as ssEPI or ssFSE sequences. The results of the latter (non-SSFP) approaches are, however, more heterogeneous, which may be explained by the fact that the image contrast depends strongly on the detailed acquisition technique, i. e., on the pulse sequence type and acquisition parameters including echo time, diffusion weighting, fat suppression, and others.

Many studies based on non-SSFP DWI techniques describe malignant lesions in diffusion-weighted images as predominantly hyperintense relative to normal-appearing vertebral bone marrow (e. g., 62, 64, 66–68, 79, 97, 109), but the reliable differentiation from benign (osteoporotic) fractures remains difficult because of the inconsistent results found for the latter. Some studies report a good differentiation based on hypointense signal of benign lesions in DWI (e. g., 66, 79, 112), while others find either varying contrasts for these lesions (94, 97) or a similar contrast as for malignant lesions (68, 94, 95, 109). Sung et al. described most benign fractures as "hyperintense relative to normal bone marrow and hypointense relative to spinal cord", which enables a differentiation from malignant fractures, which are found to be predominantly "hyperintense relative to spinal cord" (62). Generally, hypointense lesion signal appears to be a reasonably specific indicator for benign lesion etiology with, however, only moderate sensitivity (102).

The visual contrast in all these qualitative diffusion-weighting studies (with either conventional ssEPI and ssFSE sequences or with diffusion-weighted SSFP acquisitions) is usually explained by the differences of the ADC described in the previous section: Osteoporotic fractures have higher ADCs than neoplastic lesions; hence, the signal attenuation of osteoporotic fractures due to the applied diffusion weighting is stronger and they appear darker. However, the visual contrast relative to normal appearing bone marrow cannot be easily explained using the ADC alone: The ADC of normal bone marrow is substantially lower than the ADC of both kinds of lesions and the image intensity could therefore be erroneously expected to be highest in normal bone marrow. In reality, however, normal bone marrow shows low to intermediate signal intensities in DWI. This low signal is caused by a combination of reduced water content (in particular, if the fat signal is suppressed), shorter transverse relaxation times ($T_2$) than in the lesion, and very short $T_2^*$ relaxation times. Obviously, the exact resulting signal in vertebral bone marrow depends on the sequence parameters used for DWI, in particular on the echo time and the application of fat suppression pulses.

A detailed quantitative analysis of the lesion contrast in diffusion-weighting SSFP acquisitions was recently published by Biffar et al. based on Eq. (2) shown above (32). To calculate the diffusion-weighted SSFP signal quantitatively, mean values of the ADC and relaxation times ($T_1$, $T_2$, and $T_2^*$) were required for all considered tissues (i. e., for normal-appearing bone marrow and for both types of lesions). In particular, since bone marrow consists of comparable amounts of signal-generating fat and water, these parameters need to be known independently for the fat and the water component together with the relative fat fraction. Combining all these data, the influence of all individual parameters on the observed tissue contrast can be calculated. As a result, it turned out that the SSFP contrast is caused predominantly by the differences (between the patients with benign and the ones with malignant lesions) of fat fractions and of $T_2^*$ in both the normal appearing bone marrow and in the vertebral lesions. The existing significant differences of the ADC, on the other hand, contribute only to a low degree to the image contrast in diffusion-weighted SSFP MRI (32).

A very important prerequisite to obtain this SSFP contrast behavior is that the fat and water signals in normal appearing bone marrow cancel to a certain degree and, thus, reduce the MRI signal of the bone marrow. This requires an opposed-phase (or at least strongly out-of phase) condition during the signal readout of the SSFP sequence, which is possible since the SSFP-readout is shifted relative to the generic spin-echo position and different phases are accumulated by the fat and water component. Consequently, the (reversed) echo time of the pulse sequence, i. e., the interval between the center of the acquired echo and the subsequent radio-frequency pulse, is a particularly relevant parameter for the contrast of diffusion-weighted SSFP acquisitions; approximately opposed fat and water phases are found for echo times of about 7 ms (or, e. g., 2.4 or 11.6 ms) at a field strength of 1.5 T.

## Conclusions

Vertebral bone marrow has some unique magnetic resonance and tissue properties that need to be taken into account in diffusion MRI of the spinal column. Due to both the spongy microstructure of the trabecular bone and the neighborhood of the lung, soft tissue, or large vessels, substantial magnetic susceptibility variations occur which severely reduce the transverse relaxation time $T_2^*$ and complicate MRI in particular with echoplanar imaging techniques. In addition, the MR signal of bone marrow contains water and fat contributions of comparable magnitude, if MRI techniques without fat suppression are used. Finally, the diffusion coefficient of the water in bone marrow is low ($\lesssim 0.6 \times 10^{-3}\,\mathrm{mm^2/s}$) compared to almost all other tissues, i. e., a precise ADC measurement requiring a sufficient diffusion attenuation is inherently difficult.

Only after recent technical advances in the implementa-

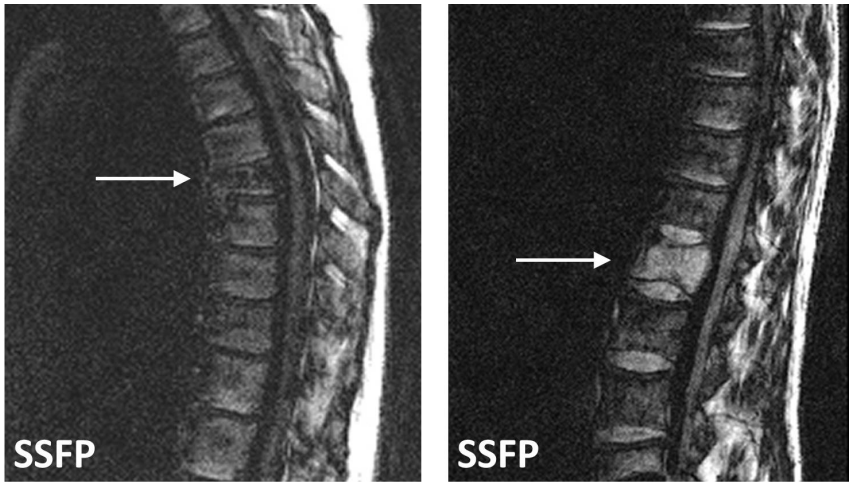


Figure 8: Diffusion-weighted SSFP acquisitions of a benign and a malignant vertebral bone marrow lesion (same patients as in Figs. 3 and 4). The osteoporotic fracture is hypointense relative to the normal-appearing vertebral bone marrow, while the metastatic lesion appears hyperintense.

tion of echoplanar imaging sequences (including improved gradient systems, parallel imaging, dynamic shimming etc.), sagittal MRI of the spine with ssEPI techniques became reasonably robust. Nevertheless, alternative diffusion-weighting pulse sequence such as single-shot fast-spin-echo sequences or segmented EPI techniques are still important alternatives for quantitative DWI of the vertebral bone marrow.

Clinically, diffusion-weighted MRI of the vertebral bone marrow is an important tool particularly for the differentiation of benign (osteoporotic) and malignant vertebral compression fractures. Numerous studies demonstrated that the average ADC of osteoporotic fractures is significantly greater than the ADC of malignant fractures or neoplastic bone marrow lesions. In addition to quantitative ADC measurements, qualitative evaluation of the lesion contrast in diffusion-weighted MRI of the vertebral column has been shown to be valuable for the differentiation of lesion etiology: A very good lesion differentiation can be achieved particularly with diffusion-weighted steady-state free precession sequences, which depict malignant lesions hyperintense relative to normal-appearing vertebral bone marrow in contrast to hypointense or isointense osteoporotic lesions.

In summary, DWI of the vertebral bone marrow is technically demanding, but – if performed with adequate techniques and caution – clinically valuable in particular for the differential diagnosis of vertebral lesions.

## References

[1] Huisman TA, Bosemani T, Poretti A. Diffusion Tensor Imaging for Brain Malformations: Does It Help? *Neuroimaging Clin. N. Am.* 2014; **24**: 619–637.

[2] Lerner A, Mogensen MA, Kim PE, Shiroishi MS, Hwang DH, Law M. Clinical applications of diffusion tensor imaging. *World Neurosurg* 2014; **82**: 96–109.

[3] Cochrane CJ, Ebmeier KP. Diffusion tensor imaging in parkinsonian syndromes: a systematic review and meta-analysis. *Neurology* 2013; **80**: 857–864.

[4] Fung SH, Roccatagliata L, Gonzalez RG, Schaefer PW. MR diffusion imaging in ischemic stroke. *Neuroimaging Clin. N. Am.* 2011; **21**: 345–377.

[5] Maier SE, Sun Y, Mulkern RV. Diffusion imaging of brain tumors. *NMR Biomed* 2010; **23**: 849–864.

[6] Moore WA, Khatri G, Madhuranthakam AJ, Sims RD, Pedrosa I. Added value of diffusion-weighted acquisitions in MRI of the abdomen and pelvis. *AJR Am J Roentgenol* 2014; **202**: 995–1006.

[7] Nguyen TL, Soyer P, Fornes P, Rousset P, Kianmanesh R, Hoeffel C. Diffusion-weighted MR imaging of the rectum: Clinical applications. *Crit. Rev. Oncol. Hematol.* 2014; **92**: 279–295.

[8] Subhawong TK, Jacobs MA, Fayad LM. Insights into quantitative diffusion-weighted MRI for musculoskeletal tumor imaging. *AJR Am J Roentgenol* 2014; **203**: 560–572.

[9] Tamada T, Sone T, Jo Y, Yamamoto A, Ito K. Diffusion-weighted MRI and its role in prostate cancer. *NMR Biomed* 2014; **27**: 25–38.

[10] Li B, Li Q, Chen C, Guan Y, Liu S. A systematic review and meta-analysis of the accuracy of diffusion-weighted MRI in the detection of malignant pulmonary nodules and masses. *Acad Radiol* 2014; **21**: 21–29.

[11] Thomassin-Naggara I, De Bazelaire C, Chopier J, Bazot M, Marsault C, Trop I. Diffusion-weighted MR imaging of the breast: advantages and pitfalls. *Eur J Radiol* 2013; **82**: 435–443.

[12] Tanenbaum LN. Clinical applications of diffusion imaging in the spine. *Magn Reson Imaging Clin N Am* 2013; **21**: 299–320.

[13] Dietrich O, Biffar A, Reiser MF, Baur-Melnyk A. Diffusion-weighted imaging of bone marrow. *Semin Musculoskelet Radiol* 2009; **13**: 134–144.

[14] Steven AJ, Zhuo J, Melhem ER. Diffusion kurtosis imaging: an emerging technique for evaluating the microstructural environment of the brain. *AJR Am J Roentgenol* 2014; **202**: 26–33.

[15] Takahara T, Kwee TC. Low b-value diffusion-weighted imaging: emerging applications in the body. *J Magn Reson Imaging* 2012; **35**: 1266–1273.

[16] Koh DM, Collins DJ, Orton MR. Intravoxel incoherent motion in body diffusion-weighted MRI: reality and challenges. *AJR Am J Roentgenol* 2011; **196**: 1351–1361.

[17] Gore JC, Xu J, Colvin DC, Yankeelov TE, Parsons EC, Does MD. Characterization of tissue structure at varying length scales using temporal diffusion spectroscopy. *NMR Biomed* 2010; **23**: 745–756.

[18] Lazar M. Mapping brain anatomical connectivity using white matter tractography. *NMR Biomed* 2010; **23**: 821–835.

[19] Hahn EL. Spin echoes. *Phys. Rev.* 1950; **80**: 580–594.

[20] Stejskal EO, Tanner JE. Spin diffusion measurements: Spin echoes in the presence of a time-dependent field gradient. *J. Chem. Phys.* 1965; **42**: 288–292.

[21] Taylor DG, Bushell MC. The spatial mapping of translational diffusion coefficients by the NMR imaging technique. *Phys Med Biol* 1985; **30**: 345–349.

[22] Le Bihan D, Breton E, Lallemand D, Grenier P, Cabanis E, Laval-Jeantet M. MR imaging of intravoxel incoherent motions: application to diffusion and perfusion in neurologic disorders. *Radiology* 1986; **161**: 401–407.

[23] Dietrich O. Diffusion-weighted imaging and diffusion tensor imaging. In: Magnetic Resonance Tomography, Reiser MF, Semmler W, Hricak H, eds., pp. 130–152. Berlin, Heidelberg, New York: Springer, 2008.

[24] Pfeuffer J, Flögel U, Dreher W, Leibfritz D. Restricted diffusion and exchange of intracellular water: theoretical modelling and diffusion time dependence of 1H NMR measurements on perfused glial cells. *NMR Biomed* 1998; **11**: 19–31.

[25] Sen PN. Time-dependent diffusion coefficient as a probe of geometry. *Conc. Magn. Reson. A* 2004; **23A**: 1–21.

[26] Dietrich O, Hubert A, Heiland S. Imaging cell size and permeability in biological tissue using the diffusion-time dependence of the apparent diffusion coefficient. *Phys Med Biol* 2014; **59**: 3081–3096.

[27] Platzer W. Color Atlas of Human Anatomy. Volume 1. Locomotor System. Stuttgart, New York: Georg Thieme Verlag, 2009, 6th revised and enlarged edition.

[28] Bartl R. Histology of normal bone and bone marrow, and their main disorders. In: Magnetic Resonance Imaging of the Bone Marrow, Baur-Melnyk A, ed., pp. 3–20. Berlin, Heidelberg: Springer, 2013.

[29] Issever AS, Link TM, Kentenich M, Rogalla P, Schwieger K, Huber MB, Burghardt AJ, Majumdar S, Diederichs G. Trabecular bone structure analysis in the osteoporotic spine using a clinical in vivo setup for 64-slice MDCT imaging: comparison to microCT imaging and microFE modeling. *J. Bone Miner. Res.* 2009; **24**: 1628–1637.

[30] Yeni YN, Zelman EA, Divine GW, Kim DG, Fyhrie DP. Trabecular shear stress amplification and variability in human vertebral cancellous bone: relationship with age, gender, spine level and trabecular architecture. *Bone* 2008; **42**: 591–596.

[31] De Santis S, Rebuzzi M, Di Pietro G, Fasano F, Maraviglia B, Capuani S. In vitro and in vivo MR evaluation of internal gradient to assess trabecular bone density. *Phys Med Biol* 2010; **55**: 5767–5785.

[32] Biffar A, Baur-Melnyk A, Schmidt GP, Reiser MF, Dietrich O. Quantitative analysis of the diffusion-weighted steady-state free precession signal in vertebral bone marrow lesions. *Invest Radiol* 2011; **46**: 601–609.

[33] Kühn JP, Hernando D, Meffert PJ, Reeder S, Hosten N, Laqua R, Steveling A, Ender S, Schröder H, Pillich DT. Proton-density fat fraction and simultaneous R2* estimation as an MRI tool for assessment of osteoporosis. *Eur Radiol* 2013; **23**: 3432–3439.

[34] Poon CS, Doumanian J, Sze G, Johnson M, Johnson CE. Spine and spinal canal. Extradural diseases of the spine. In: Magnetic Resonance Tomography, Reiser MF, Semmler W, Hricak H, eds., pp. 536–589. Berlin, Heidelberg: Springer, 2008.

[35] Dietrich O. Techniques for diffusion and perfusion assessment in bone-marrow MRI. In: Magnetic Resonance Imaging of the Bone Marrow, Baur-Melnyk A, ed., pp. 339–354. Berlin, Heidelberg: Springer, 2013.

[36] Raya JG, Dietrich O, Reiser MF, Baur-Melnyk A. Methods and applications of diffusion imaging of vertebral bone marrow. *J Magn Reson Imaging* 2006; **24**: 1207–1220.

[37] Dietrich O, Biffar A, Baur-Melnyk A, Reiser MF. Technical aspects of MR diffusion imaging of the body. *Eur J Radiol* 2010; **76**: 314–322.

[38] Dietrich O, Baur-Melnyk A. Diffusion-weighted MR imaging of the bone marrow and the spine. In: Extra-cranial applications of diffusion-weighted MRI, Taouli B, ed., pp. 144–161. Cambridge: Cambridge University Press, 2011.

[39] Merboldt KD, Hanicke W, Frahm J. Self-diffusion NMR imaging using stimulated echoes. *J Magn Reson* 1985; **64**: 479–486.

[40] Gudbjartsson H, Maier SE, Mulkern RV, Morocz IA, Patz S, Jolesz FA. Line scan diffusion imaging. *Magn Reson Med* 1996; **36**: 509–519.

[41] Raya JG, Horng A, Dietrich O, Krasnokutsky S, Beltran LS, Storey P, Reiser MF, Recht MP, Sodickson DK, Glaser C. Articular cartilage: in vivo diffusion-tensor imaging. *Radiology* 2012; **262**: 550–559.

[42] Turner R, Le Bihan D, Maier J, Vavrek R, Hedges LK, Pekar J. Echo-planar imaging of intravoxel incoherent motion. *Radiology* 1990; **177**: 407–414.

[43] Stehling MK, Turner R, Mansfield P. Echo-planar imaging: magnetic resonance imaging in a fraction of a second. *Science* 1991; **254**: 43–50.

[44] Pruessmann KP, Weiger M, Scheidegger MB, Boesiger P. SENSE: sensitivity encoding for fast MRI. *Magn Reson Med* 1999; **42**: 952–962.

[45] Griswold MA, Jakob PM, Heidemann RM, Nittka M, Jellus V, Wang J, Kiefer B, Haase A. Generalized autocalibrating partially parallel acquisitions (GRAPPA). *Magn Reson Med* 2002; **47**: 1202–1210.

[46] Bammer R, Auer M, Keeling SL, Augustin M, Stables LA, Prokesch RW, Stollberger R, Moseley ME, Fazekas F. Diffusion tensor imaging using single-shot SENSE-EPI. *Magn Reson Med* 2002; **48**: 128–136.

[47] Jaermann T, Crelier G, Pruessmann KP, Golay X, Netsch T, van Muiswinkel AM, Mori S, van Zijl PC, Valavanis A, Kollias S, Boesiger P. SENSE-DTI at 3 T. *Magn Reson Med* 2004; **51**: 230–236.

[48] Lee SK, Tan ET, Govenkar A, Hancu I. Dynamic slice-dependent shim and center frequency update in 3 T breast diffusion weighted imaging. *Magn Reson Med* 2014; **71**: 1813–1818.

[49] Butts K, Pauly J, de Crespigny A, Moseley M. Isotropic diffusion-weighted and spiral-navigated interleaved EPI for routine imaging of acute stroke. *Magn Reson Med* 1997; **38**: 741–749.

[50] Brockstedt S, Moore JR, Thomsen C, Holtas S, Stahlberg F. High-resolution diffusion imaging using phase-corrected segmented echo-planar imaging. *Magn Reson Imaging* 2000; **18**: 649–657.

[51] Holdsworth SJ, Skare S, Newbould RD, Guzmann R, Blevins NH, Bammer R. Readout-segmented EPI for rapid high resolution diffusion imaging at 3 T. *Eur J Radiol* 2008; **65**: 36–46.

[52] Porter DA, Heidemann RM. High resolution diffusion-weighted imaging using readout-segmented echo-planar imaging, parallel imaging and a two-dimensional navigator-based reacquisition. *Magn Reson Med* 2009; **62**: 468–475.

[53] Norris DG, Bornert P, Reese T, Leibfritz D. On the application of ultra-fast RARE experiments. *Magn Reson Med* 1992; **27**: 142–164.

[54] Lovblad KO, Jakob PM, Chen Q, Baird AE, Schlaug G, Warach S, Edelman RR. Turbo spin-echo diffusion-weighted MR of ischemic stroke. *AJNR Am J Neuroradiol* 1998; **19**: 201–208.

[55] Gyngell ML. The application of steady-state free precession in rapid 2DFT NMR imaging: FAST and CE-FAST sequences. *Magn Reson Imaging* 1988; **6**: 415–419.

[56] Bruder H, Fischer H, Graumann R, Deimling M. A new steady-state imaging sequence for simultaneous acquisition of two MR images with clearly different contrasts. *Magn Reson Med* 1988; **7**: 35–42.

[57] Le Bihan D. Intravoxel incoherent motion imaging using steady-state free precession. *Magn Reson Med* 1988; **7**: 346–351.

[58] Merboldt KD, Bruhn H, Frahm J, Gyngell ML, Hanicke W, Deimling M. MRI of "diffusion" in the human brain: new results using a modified CE-FAST sequence. *Magn Reson Med* 1989; **9**: 423–429.

[59] Kaiser R, Bartholdi E, Ernst RR. Diffusion and field-gradient effects in NMR Fourier spectroscopy. *J Chem Phys* 1974; **60**: 2966–2979.

[60] Wu EX, Buxton RB. Effect of diffusion on the steady-state magnetization with pulsed field gradients. *J Magn Reson* 1990; **90**: 243–253.

[61] Hillengass J, Stieltjes B, Bauerle T, McClanahan F, Heiss C, Hielscher T, Wagner-Gund B, Habetler V, Goldschmidt H, Schlemmer HP, Delorme S, Zechmann CM. Dynamic contrast-enhanced magnetic resonance imaging (DCE-MRI) and diffusion-weighted imaging of bone marrow in healthy individuals. *Acta Radiol* 2011; **52**: 324–330.

[62] Sung JK, Jee WH, Jung JY, Choi M, Lee SY, Kim YH, Ha KY, Park CK. Differentiation of acute osteoporotic and malignant compression fractures of the spine: use of additive qualitative and quantitative axial diffusion-weighted MR imaging to conventional MR imaging at 3.0 T. *Radiology* 2014; **271**: 488–498.

[63] Wan X, Wang W, Liu J, Tong T. Estimating the sample mean and standard deviation from the sample size, median, range and/or interquartile range. *BMC Med Res Methodol* 2014; **14**: 135.

[64] Herneth AM, Naude J, Philipp M, Beichel R, Trattnig S, Imhof H. [The value of diffusion-weighted MRT in assessing the bone marrow changes in vertebral metastases]. *Radiologe* 2000; **40**: 731–736.

[65] Dietrich O, Herlihy A, Dannels WR, Fiebach J, Heiland S, Hajnal JV, Sartor K. Diffusion-weighted imaging of the spine using radial k-space trajectories. *MAGMA Magn Reson Mater Phy* 2001; **12**: 23–31.

[66] Chan JH, Peh WC, Tsui EY, Chau LF, Cheung KK, Chan KB, Yuen MK, Wong ET, Wong KP. Acute vertebral body compression fractures: discrimination between benign and malignant causes using apparent diffusion coefficients. *Br J Radiol* 2002; **75**: 207–214.

[67] Byun WM, Shin SO, Chang Y, Lee SJ, Finsterbusch J, Frahm J. Diffusion-weighted MR imaging of metastatic disease of the spine: assessment of response to therapy. *AJNR Am J Neuroradiol* 2002; **23**: 906–912.

[68] Herneth AM, Philipp MO, Naude J, Funovics M, Beichel RR, Bammer R, Imhof H. Vertebral metastases: assessment with apparent diffusion coefficient. *Radiology* 2002; **225**: 889–894.

[69] Bammer R, Herneth AM, Maier SE, Butts K, Prokesch RW, Do HM, Atlas SW, Moseley ME. Line scan diffusion imaging of the spine. *AJNR Am J Neuroradiol* 2003; **24**: 5–12.

[70] Yeung DK, Wong SY, Griffith JF, Lau EM. Bone marrow diffusion in osteoporosis: evaluation with quantitative MR diffusion imaging. *J Magn Reson Imaging* 2004; **19**: 222–228.

[71] Pui MH, Mitha A, Rae WI, Corr P. Diffusion-weighted magnetic resonance imaging of spinal infection and malignancy. *J Neuroimaging* 2005; **15**: 164–170.

[72] Griffith JF, Yeung DK, Antonio GE, Wong SY, Kwok TC, Woo J, Leung PC. Vertebral marrow fat content and diffusion and perfusion indexes in women with varying bone density: MR evaluation. *Radiology* 2006; **241**: 831–838.

[73] Hatipoglu HG, Selvi A, Ciliz D, Yuksel E. Quantitative and diffusion MR imaging as a new method to assess osteoporosis. *AJNR Am J Neuroradiol* 2007; **28**: 1934–1937.

[74] Oner AY, Tali T, Celikyay F, Celik A, Le Roux P. Diffusion-weighted imaging of the spine with a non-carr-purcell-meiboom-gill single-shot fast spin-echo sequence: initial experience. *AJNR Am J Neuroradiol* 2007; **28**: 575–580.

[75] Raya JG, Dietrich O, Birkenmaier C, Sommer J, Reiser MF, Baur-Melnyk A. Feasibility of a RARE-based sequence for quantitative diffusion-weighted MRI of the spine. *Eur Radiol* 2007; **17**: 2872–2879.

[76] Byun WM, Jang HW, Kim SW, Jang SH, Ahn SH, Ahn MW. Diffusion-weighted magnetic resonance imaging of sacral insufficiency fractures: comparison with metastases of the sacrum. *Spine* 2007; **32**: E820–E824.

[77] Tang GY, Lv ZW, Tang RB, Liu Y, Peng YF, Li W, Cheng YS. Evaluation of MR spectroscopy and diffusion-weighted MRI in detecting bone marrow changes in postmenopausal women with osteoporosis. *Clin Radiol* 2010; **65**: 377–381.

[78] Eguchi Y, Ohtori S, Yamashita M, Yamauchi K, Suzuki M, Orita S, Kamoda H, Arai G, Ishikawa T, Miyagi M, Ochiai N, Kishida S, Masuda Y, Ochi S, Kikawa T, Takaso M, Aoki Y, Inoue G, Toyone T, Takahashi K. Diffusion magnetic resonance imaging to differentiate degenerative from infectious endplate abnormalities in the lumbar spine. *Spine* 2011; **36**: 198–202.

[79] Pozzi G, Garcia Parra C, Stradiotti P, Tien TV, Luzzati A, Zerbi A. Diffusion-weighted MR imaging in differentiation between osteoporotic and neoplastic vertebral fractures. *Eur Spine J* 2012; **21 Suppl 1**: S123–127.

[80] Herrmann J, Krstin N, Schoennagel BP, Sornsakrin M, Derlin T, Busch JD, Petersen KU, Graessner J, Adam G, Habermann CR. Age-related distribution of vertebral bone-marrow diffusivity. *Eur J Radiol* 2012; **81**: 4046–4049.

[81] Dutoit JC, Vanderkerken MA, Anthonissen J, Dochy F, Verstraete KL. The diagnostic value of SE MRI and DWI of the spine in patients with monoclonal gammopathy of undetermined significance, smouldering myeloma and multiple myeloma. *Eur Radiol* 2014; **24**: 2754–2765.

[82] Mulkern RV, Schwartz RB. In re: characterization of benign and metastatic vertebral compression fractures with quantitative diffusion MR imaging. *AJNR Am J Neuroradiol* 2003; **24**: 1489–1490.

[83] Dietrich O, Heiland S, Sartor K. Noise correction for the exact determination of apparent diffusion coefficients at low SNR. *Magn Reson Med* 2001; **45**: 448–453.

[84] Zhang CY, Rong R, Wang XY. Age-related changes of bone marrow of normal adult man on diffusion weighted imaging. *Chin Med Sci J* 2008; **23**: 162–165.

[85] Ueda Y, Miyati T, Ohno N, Motono Y, Hara M, Shibamoto Y, Kasai H, Kawamitsu H, Matsubara K. Apparent diffusion coefficient and fractional anisotropy in the vertebral bone marrow. *J Magn Reson Imaging* 2010; **31**: 632–635.

[86] Marchand AJ, Hitti E, Monge F, Saint-Jalmes H, Guillin R, Duvauferrier R, Gambarota G. MRI quantification of diffusion and perfusion in bone marrow by intravoxel incoherent motion (IVIM) and non-negative least square (NNLS) analysis. *Magn Reson Imaging* 2014; **32**: 1091–1096.

[87] Ohno N, Miyati T, Kasai H, Arai N, Kawano M, Shibamoto Y, Kobayashi S, Gabata T, Matsui O. Evaluation of perfusion-related and true diffusion in vertebral bone marrow: a preliminary study. *Radiol Phys Technol* 2015; **8**: 135–140.

[88] Kerttula LI, Jauhiainen JP, Tervonen O, Suramo IJ, Koivula A, Oikarinen JT. Apparent diffusion coefficient in thoracolumbar intervertebral discs of healthy young volunteers. *J Magn Reson Imaging* 2000; **12**: 255–260.

[89] Zhang W, Ma X, Wang Y, Zhao J, Zhang X, Gao Y, Li S. Assessment of apparent diffusion coefficient in lumbar intervertebral disc degeneration. *Eur Spine J* 2014; **23**: 1830–1836.

[90] Kealey SM, Aho T, Delong D, Barboriak DP, Provenzale JM, Eastwood JD. Assessment of apparent diffusion coefficient in normal and degenerated intervertebral lumbar disks: initial experience. *Radiology* 2005; **235**: 569–574.

[91] Beattie PF, Donley JW, Arnot CF, Miller R. The change in the diffusion of water in normal and degenerative lumbar intervertebral discs following joint mobilization compared to prone lying. *J Orthop Sports Phys Ther* 2009; **39**: 4–11.

[92] Niu G, Yang J, Wang R, Dang S, Wu EX, Guo Y. MR imaging assessment of lumbar intervertebral disk degeneration and age-related changes: apparent diffusion coefficient versus T2 quantitation. *AJNR Am J Neuroradiol* 2011; **32**: 1617–1623.

[93] Baur A, Stabler A, Bruning R, Bartl R, Krodel A, Reiser M, Deimling M. Diffusion-weighted MR imaging of bone marrow: differentiation of benign versus pathologic compression fractures. *Radiology* 1998; **207**: 349–356.

[94] Zhou XJ, Leeds NE, McKinnon GC, Kumar AJ. Characterization of benign and metastatic vertebral compression fractures with quantitative diffusion MR imaging. *AJNR Am J Neuroradiol* 2002; **23**: 165–170.

[95] Maeda M, Sakuma H, Maier SE, Takeda K. Quantitative assessment of diffusion abnormalities in benign and malignant vertebral compression fractures by line scan diffusion-weighted imaging. *AJR Am J Roentgenol* 2003; **181**: 1203–1209.

[96] Tang G, Liu Y, Li W, Yao J, Li B, Li P. Optimization of b value in diffusion-weighted MRI for the differential diagnosis of benign and malignant vertebral fractures. *Skeletal Radiol* 2007; **36**: 1035–1041.

[97] Balliu E, Vilanova JC, Pelaez I, Puig J, Remollo S, Barcelo C, Barcelo J, Pedraza S. Diagnostic value of apparent diffusion coefficients to differentiate benign from malignant vertebral bone marrow lesions. *Eur J Radiol* 2009; **69**: 560–566.

[98] Rumpel H, Chong Y, Porter DA, Chan LL. Benign versus metastatic vertebral compression fractures: combined diffusion-weighted MRI and MR spectroscopy aids differentiation. *Eur Radiol* 2013; **23**: 541–550.

[99] Taşkin G, İncesu K, Aslan K. The value of apparent diffusion coefficient measurements in the differential diagnosis of vertebral bone marrow lesions. *Turk J Med Sci* 2013; **43**: 379–387.

[100] Geith T, Schmidt G, Biffar A, Dietrich O, Duerr HR, Reiser M, Baur-Melnyk A. Quantitative evaluation of benign and malignant vertebral fractures with diffusion-weighted MRI: what is the optimum combination of b values for ADC-based lesion differentiation with the single-shot turbo spin-echo sequence? *AJR Am J Roentgenol* 2014; **203**: 582–588.

[101] Wonglaksanapimon S, Chawalparit O, Khumpunnip S, Tritrakarn SO, Chiewvit P, Charnchaowanish P. Vertebral body compression fracture: discriminating benign from malignant causes by diffusion-weighted MR imaging and apparent diffusion coefficient value. *J Med Assoc Thai* 2012; **95**: 81–87.

[102] Karchevsky M, Babb JS, Schweitzer ME. Can diffusion-weighted imaging be used to differentiate benign from pathologic fractures? A meta-analysis. *Skeletal Radiol* 2008; **37**: 791–795.

[103] Messiou C, Giles S, Collins DJ, West S, Davies FE, Morgan GJ, Desouza NM. Assessing response of myeloma bone disease with diffusion-weighted MRI. *Br J Radiol* 2012; **85**: e1198–1203.

[104] Razek AA, Abdalla A, Fathy A, Megahed A. Apparent diffusion coefficient of the vertebral bone marrow in children with Gaucher's disease type I and III. *Skeletal Radiol* 2013; **42**: 283–287.

[105] Baur A, Huber A, Ertl-Wagner B, Durr R, Zysk S, Arbogast S, Deimling M, Reiser M. Diagnostic value of increased diffusion weighting of a steady-state free precession sequence for differentiating acute benign osteoporotic fractures from pathologic vertebral compression fractures. *AJNR Am J Neuroradiol* 2001; **22**: 366–372.

[106] Baur A, Huber A, Durr HR, Nikolaou K, Stabler A, Deimling M, Reiser M. [Differentiation of benign osteoporotic and neoplastic vertebral compression fractures with a diffusion-weighted, steady-state free precession sequence]. *Rofo* 2002; **174**: 70–75.

[107] Abanoz R, Hakyemez B, Parlak M. [Diffusion-weighted imaging of acute vertebral compression: Differential diagnosis of benign versus malignant pathologic fractures]. *Tani Girisim Radyol* 2003; **9**: 176–183.

[108] Bhugaloo A, Abdullah B, Siow Y, Ng Kh. Diffusion weighted MR imaging in acute vertebral compression fractures: differentiation between malignant and benign causes. *Biomed Imaging Interv J* 2006; **2**: e12.

[109] Geith T, Schmidt G, Biffar A, Dietrich O, Durr HR, Reiser M, Baur-Melnyk A. Comparison of qualitative and quantitative evaluation of diffusion-weighted MRI and chemical-shift imaging in the differentiation of benign and malignant vertebral body fractures. *AJR Am J Roentgenol* 2012; **199**: 1083–1092.

[110] Castillo M, Arbelaez A, Smith JK, Fisher LL. Diffusion-weighted MR imaging offers no advantage over routine noncontrast MR imaging in the detection of vertebral metastases. *AJNR Am J Neuroradiol* 2000; **21**: 948–953.

[111] Hacklander T, Scharwachter C, Golz R, Mertens H. [Value of diffusion-weighted imaging for diagnosing vertebral metastases due to prostate cancer in comparison to other primary tumors]. *Rofo* 2006; **178**: 416–424.

[112] Spuentrup E, Buecker A, Adam G, van Vaals JJ, Guenther RW. Diffusion-weighted MR imaging for differentiation of benign fracture edema and tumor infiltration of the vertebral body. *AJR Am J Roentgenol* 2001; **176**: 351–358.